AD-A189 695 PARTICLE BEAM ALIGNMENT SYSTEM FOR SINGLE EVENT UPSET - 1/1
VAN DE GRAAFF EXPERIMENTS(U) PHYSICAL SCIENCES INC
ALEXANDRIA VA M R CORSON ET AL. 01 JUN 87 PSI-9898
UNCLASSIFIED N00014-83-C-2255 F/G 20/7 NL

END
DATE FILMED
4 88

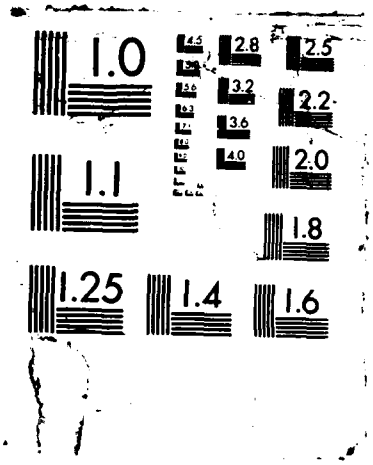
1.0
1.1
1.25
1.4
1.6
1.8
2.0
2.2
2.5
2.8
3.2
3.6
4.0

PSI-9898
TR-683

PARTICLE BEAM ALIGNMENT SYSTEM

FOR

SINGLE EVENT UPSET - VAN DE GRAAFF EXPERIMENTS

Final Report

Contract Number: N00014-83-C-2255

Michael R. Corson
Jack A. McKay
James H. McDermott

Submitted to:

The U.S. Naval Research Laboratory
Washington, DC

1 June 1987

PHYSICAL SCIENCES INC.
RESEARCH PARK, ANDOVER, MA 01810

603 KING STREET, ALEXANDRIA, VA 22314

PSI-9898
TR-683

PARTICLE BEAM ALIGNMENT SYSTEM

FOR

SINGLE EVENT UPSET - VAN DE GRAAFF EXPERIMENTS

Final Report
Contract Number: N00014-83-C-2255

Michael R. Corson
Jack A. McKay
James H. McDermott

Submitted to:

The U.S. Naval Research Laboratory
Washington, DC

1 June 1987

TABLE OF CONTENTS

1.0 INTRODUCTION

This report documents the design and operation of the particle beam alignment system developed by PSI for single event upset - Van de Graaff experiments. This system is designed to provide a faster and more accurate optical alignment of the pinhole and the device under test. In this alignment system a laser beam is focused on the device under test, and the pinhole is then aligned with the laser beam using an electronic display. In this way the pinhole is aligned over the device under test.

The alignment system consists of three main components:

1. A beam expander for the He-Ne laser which was previously used for pinhole alignment, and neutral density filters to attenuate the laser beam when necessary

2. A new flange for the sample chamber incorporating a calibrated x-y translation stage for the pinhole, and a calibrated x-y translation stage carrying a quadrant photodiode

3. An amplifier and display module to display the output of the photodiode.

The beam expander is used so that the laser beam can be focused to a small Gaussian spot on the device under test. This spot is substantially smaller and more intense than the laser spot without a beam expander, to allow a more precise alignment. The silicon photodiode and display are then used to center the pinhole in the laser beam, so that the pinhole is aligned over the device under test.

The operation of the alignment system is described in Section 2. The electronic amplifier and display module are described in Section 3. The radius and depth of focus of the laser spot are computed in Section 4, and measurements of the beam profile are presented. An article on the optics of laser resonators and laser beams is reproduced in Appendix 1. The principle of operation of the quadrant photodiode used in the alignment system, and a dimensional diagram of the quadrant photodiode, are reproduced in Appendix 2.

2.0 SINGLE EVENT UPSET - VAN DE GRAAFF ALIGNMENT SYSTEM

The pinhole alignment device for the single event upset - Van de Graaff system is shown schematically in Figure 1. The laser beam from the beam expander enters the particle beam path through a window in the side of the vacuum line. Inside the vacuum line the laser beam is reflected at a right angle so that it travels down the center of the vacuum line into the sample chamber. The sample chamber contains the pinhole, a silicon photodiode, and the device under test. The alignment procedure is detailed below.

2.1 Pinhole Alignment Procedure

The procedure for aligning the pinhole and the device under test, using the new alignment system, is carried out with the following steps.

1. Align the beam expander axis with the laser axis, so that the expanded laser beam is symmetrical as viewed on a screen directly in front of the beam expander

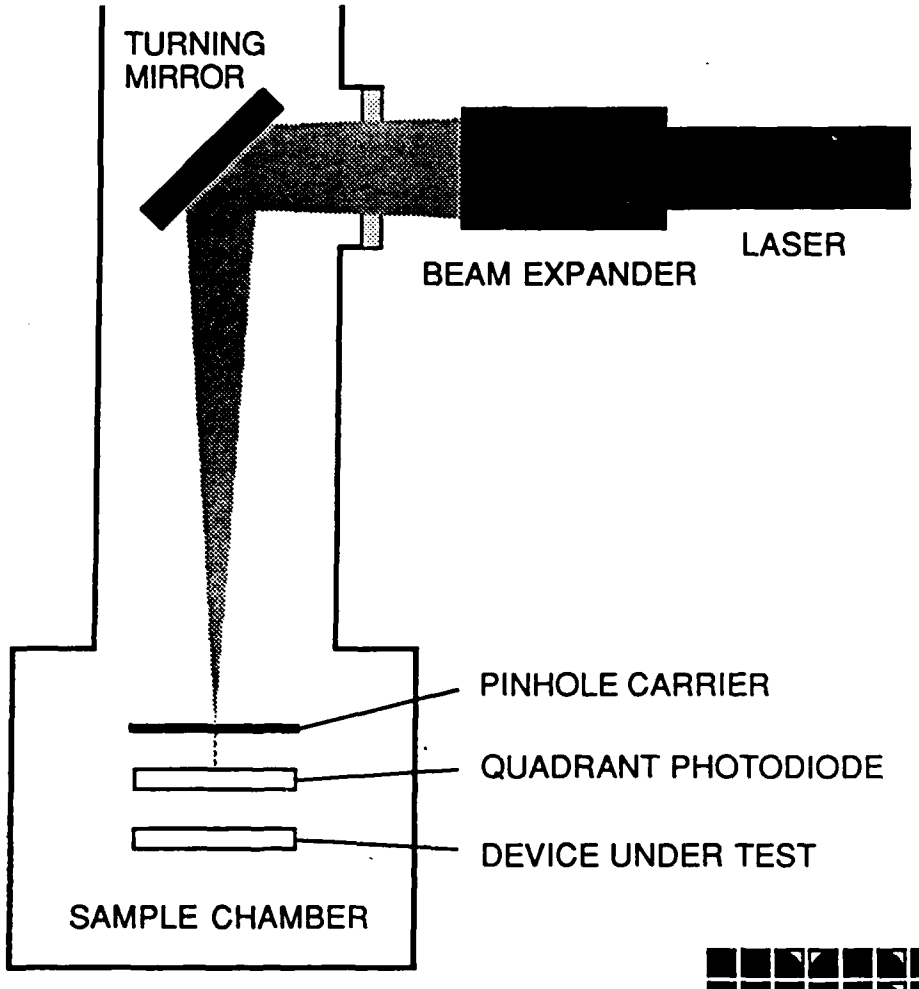

Physical Sciences Inc.
Washington Operations

Figure 1. Schematic representation of the beam alignment device for single event upset - Van de Graaff experiments.

2. Set up the laser and beam expander so that the laser beam enters the particle beam line, and is reflected by a mirror so that the axis of the laser beam and coincides with the axis of the particle beam.

3. Focus the beam expander so that the laser spot at the position of the device under test is minimum size.

4. Center the integrated circuit structure of interest in the focused laser beam using the observing microscope . The laser spot is intense, and scattered light can obscure the central spot. Neutral density filters can be placed in the laser beam to attenuate the spot intensity as needed.

5. Move the pinhole into the laser beam, using the calibrated motion controls of the x-y stage for the pinhole. Move the photodiode into the beam path behind the pinhole.

6. Adjust the position of the pinhole to maximize the laser light passing through the pinhole, using the quadrant photodiode as a simple photodiode to measure the total light passing through the pinhole. The photocell display should be set to "sum" for this step. Since the focused laser spot is Gaussian, the light passing through the pinhole peaks rather sharply when the pinhole is centered in the laser beam.

7. Move the photodiode out of the beam path. This completes the alignment procedure.

2.2 Photodiode Quadrant Mode

The quadrant photodiode contains four anodes. Two of the anodes are located on horizontally opposite sides of the diode's active area, and two are located on vertically opposite sides. The horizontally opposite pair is connected to the differential inputs of an amplifier, and the output of the amplifier is shown on a zero center meter on the electronic display module. The vertically opposite pair is similarly connected to an amplifier and zero center meter. When the laser spot is centered on the quadrant photodiode, both meters will be centered.

The quadrant photodiode and its calibrated x-y translation stage can be used to measure the position of the laser spot in the sample chamber. This can be useful when moving the pinhole into the laser spot as in step 5 above. The focused laser spot is small, and unless the pinhole is within approximately 100 microns of the spot center, virtually no light passes through the pinhole. Therefore, if the position of the pinhole is not known and cannot be determined by looking at the pinhole carrier through the observing microscope, a search procedure may be necessary to move the pinhole into the laser beam.

Using the quadrant photodiode to locate the laser beam eliminates the need for a time-consuming search to find the laser beam with the pinhole. Of course, it is necessary to find the relative positions of the center of the quadrant photodiode and the pinhole once, after which no further searching is necessary.

3.0 AMPLIFIER AND DISPLAY MODULE

A schematic diagram of the measurement electronics is shown in Figure 2. As shown on the figure, the quadrant photodiode has four anodes, pins 1, 2, 4, and 5. When the 5 pole 2 position rotary switch is set to the right, pins 1 and 4 are connected to the anodes on the horizontally opposite sides of the active area, and pins 2 and 5 are connected to the anodes of the vertically opposite sides of the active area. The upper FET input dual operational amplifier, type AD647L, converts the two photocurrents from pins 1 and 4 into two voltages which are applied to the inputs of the upper instrumentation amplifier type AD524C. A null at the output of this instrumentation amplifier, seen on the meter connected to its output, signifies that the laser spot is centered horizontally on the active area of the quadrant photodiode. Note that the rotary switch also short circuits the 10 K variable resistor in the feedback loop of the top operational amplifier, which is not needed in this mode. The lower dual operational amplifier and instrumentation amplifier allow vertical centering of the laser spot on the quadrant photodiode. Therefore, by nulling the two meters the laser spot can be centered on the quadrant photodiode.

When the rotary switch is set to the left, all four anodes of the quadrant photodiode are connected together, so that the detector operates as a simple photodiode. The four anodes are connected to the input of the upper operational amplifier. The inputs of the other operational amplifiers are disconnected, which in their current-to-voltage conversion mode simply sets their outputs to zero. Therefore, the upper meter displays the total output of the quadrant photodiode, so that the pinhole can be centered in the laser beam. Note that in this mode the 10 K variable resistor in added to the current-to-voltage conversion resistance for the upper operational amplifier. This is done to provide additional gain, because only a limited amount of light passes through the pinhole, as well as provide variable gain which is convenient for the final centering operation.

4.0 DIMENSIONS OF THE FOCUSED LASER SPOT

The accuracy of the single event upset - Van de Graaff alignment system is partially determined by the size of the laser spot used for the alignment. The anticipated size and depth of focus of the laser spot are computed in Section 4.1, and measurements of the size and intensity profile of the laser spot are presented in Section 4.2.

4.1 Computed Radius and Depth of Focus of the Laser Spot

A discussion of the propagation of laser beams is included in Appendix 1, and the results presented in that appendix will be used to compute the size and depth of focus of the laser spot. The radius and depth of focus of the laser spot are determined by the radius of the beam waist in the laser cavity and the characteristics of the beam expander. Assuming a confocal resonator typical of this type of laser, the formula for the waist radius is given in the text following Equation 3 in Appendix 1. The waist radius w at the 13.5 per cent intensity point is

$$w = [\ \lambda * L / 6.28\ ]^{1/2}$$

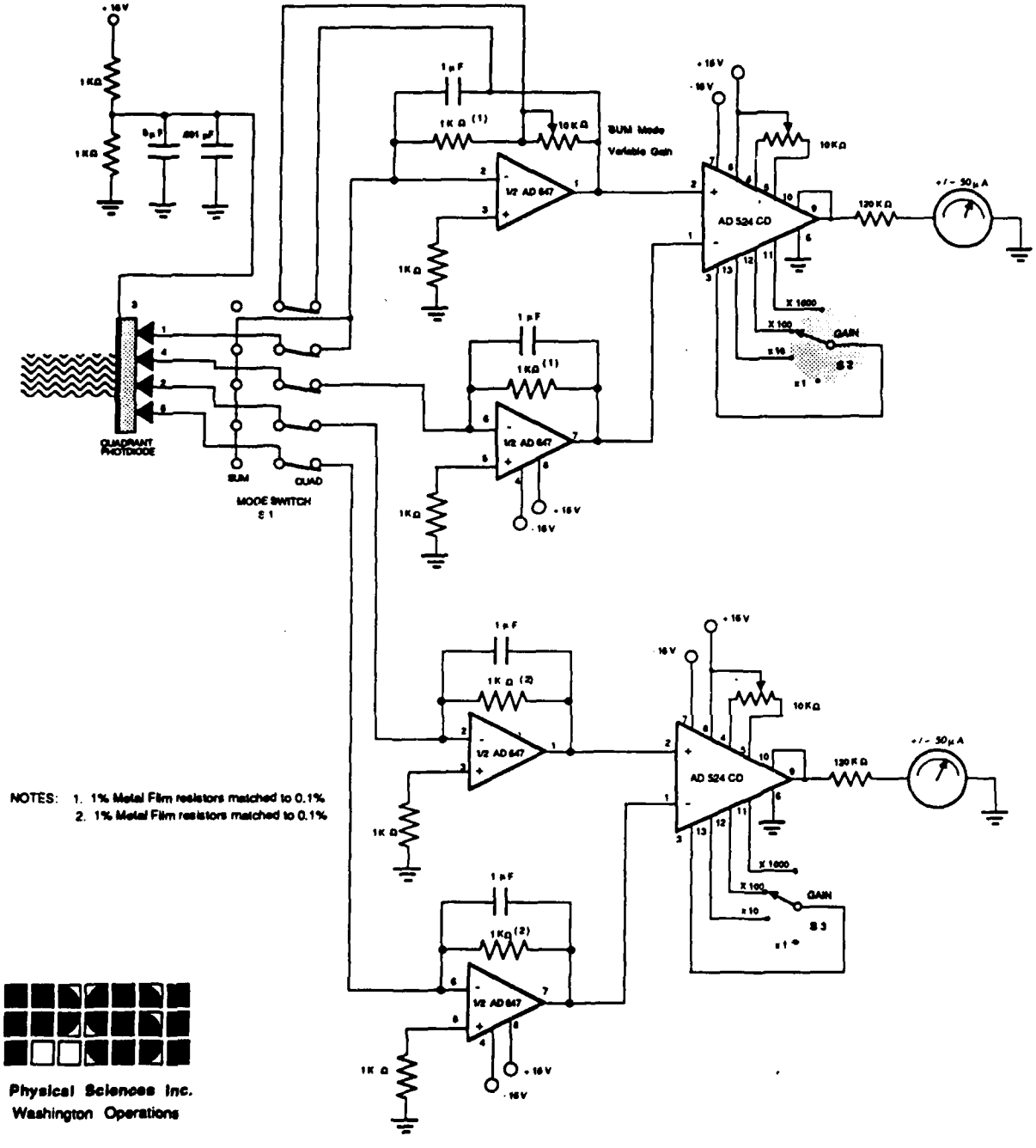

NOTES: 1. 1% Metal Film resistors matched to 0.1%
2. 1% Metal Film resistors matched to 0.1%

Physical Sciences Inc.
Washington Operations

Figure 2. Schematic diagram of the amplifier and display electronics.

where lambda is the laser wavelength, 6.33E-5 cm, and L is the laser cavity length, specified by the manufacturer to be 23 cm. This yields a waist radius of 1.5E-2 cm.

The laser spot focused on the device under test is the waist of the beam exiting the beam expander. The waist radius w of this beam is computed using Equation 10 in Appendix 1,

$$w = lambda * f / (3.14 * wl)$$

where in this formula, f is the distance from the beam expander to the focused spot, and wl is the waist radius of the beam inside the laser cavity multiplied by the beam expansion ratio. The distance from the beam expander to the focused spot is 126 cm. The expansion ratio of the beam expander is 20, so that wl = 1.5E-2 * 20 = 0.3 cm. Therefore, we find the computed radius of the focused laser spot to be 8.5E-3 cm at the 13.5 per cent intensity point. The diameter is then 1.7E-2 cm, or 170 microns.

The depth of focus of the laser spot is computed using Equation 11 in Appendix 1. The depth of focus d is given by

$$d = +/- (3.14 * w * w / lambda) * [rho * rho - 1]^{1/2}$$

where w is the radius of the focused spot and rho is the acceptable increase in spot size; for example, a 50 per cent increase in the radius of the spot corresponds to rho = 1.5. Assuming rho = 1.5 and using the computed value of the radius of the focused spot, w = 8.5E-3, the computed depth of focus is +/- 4.0 cm. The total depth of focus is therefore 8 cm.

4.2 Measurement of the Focused Laser Spot Profile

The profile of the focused laser spot was measured in the laboratory to determine its suitability for the alignment system. For these measurements the beam from the laser was directed over an optical path equivalent to the optical path in the Van de Graaff beam line. In particular, the expanded laser beam was directed at a 45 degree angle of incidence onto a mirror of the type used as the beam director in the Van de Graaff beam line. The focused laser spot then fell onto a disk containing a 10 micron diameter pinhole. The optical path length from the beam expander to the pinhole disk was 126 cm. For some measurements the glass window through which the laser beam must pass to enter the Van de Graaff particle beam line was placed at the appropriate position in the optical path. For other measurements this glass window was not used.

To measure the profile of the laser spot, the quadrant photodiode was positioned behind the pinhole and the pinhole was scanned horizontally and vertically across the laser spot in 10 micron steps. The total laser light passing through the pinhole and reaching the photodiode was recorded at each step, using the photodiode display in the "sum" mode. The resulting profiles show the intensity profile of the laser spot.

The results of these measurements are shown in Figures 3 through 6. Figures 3 and 4 show the spot profile without and with the window, respectively. The optics were then intentionally misaligned and realigned, and the measurements

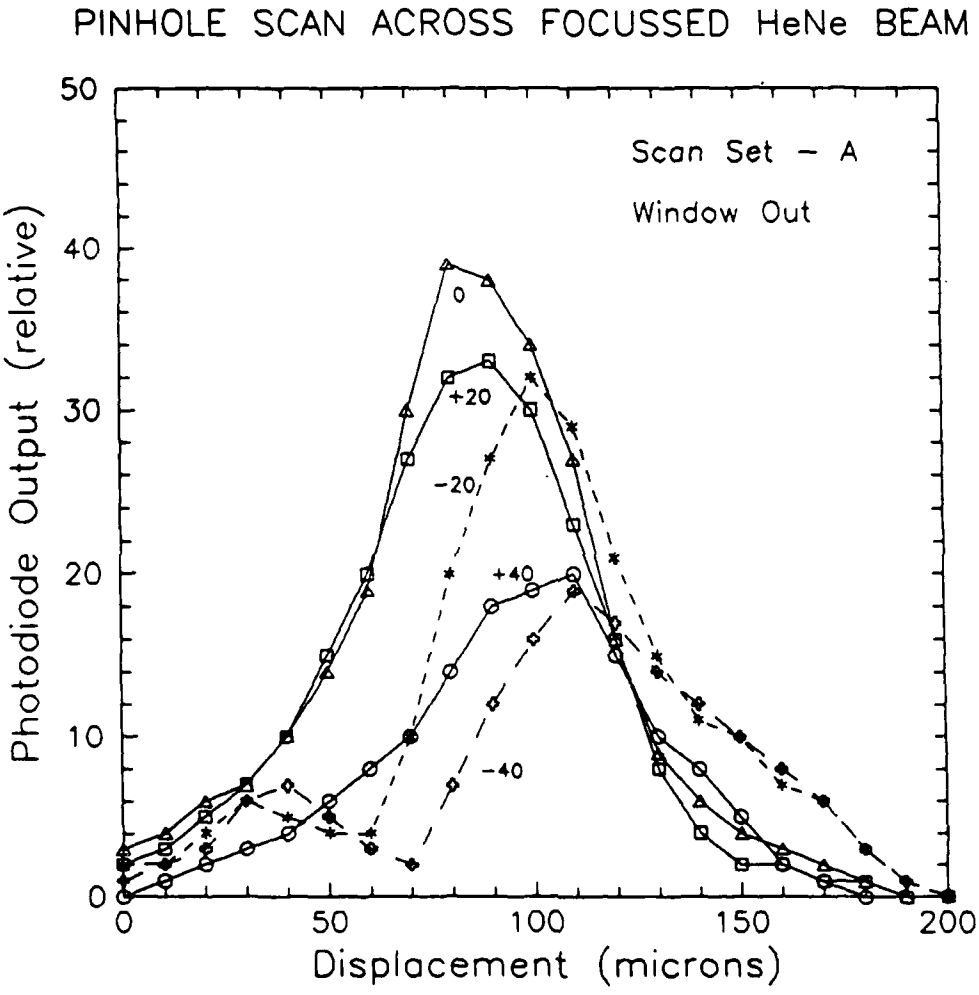

Figure 3. Intensity profile of focused laser spot with no window in the laser beam path - first alignment. Horizontal displacement is shown on the horizontal axis. Vertical displacement in 20 micron increments is shown by the individual labeled curves.

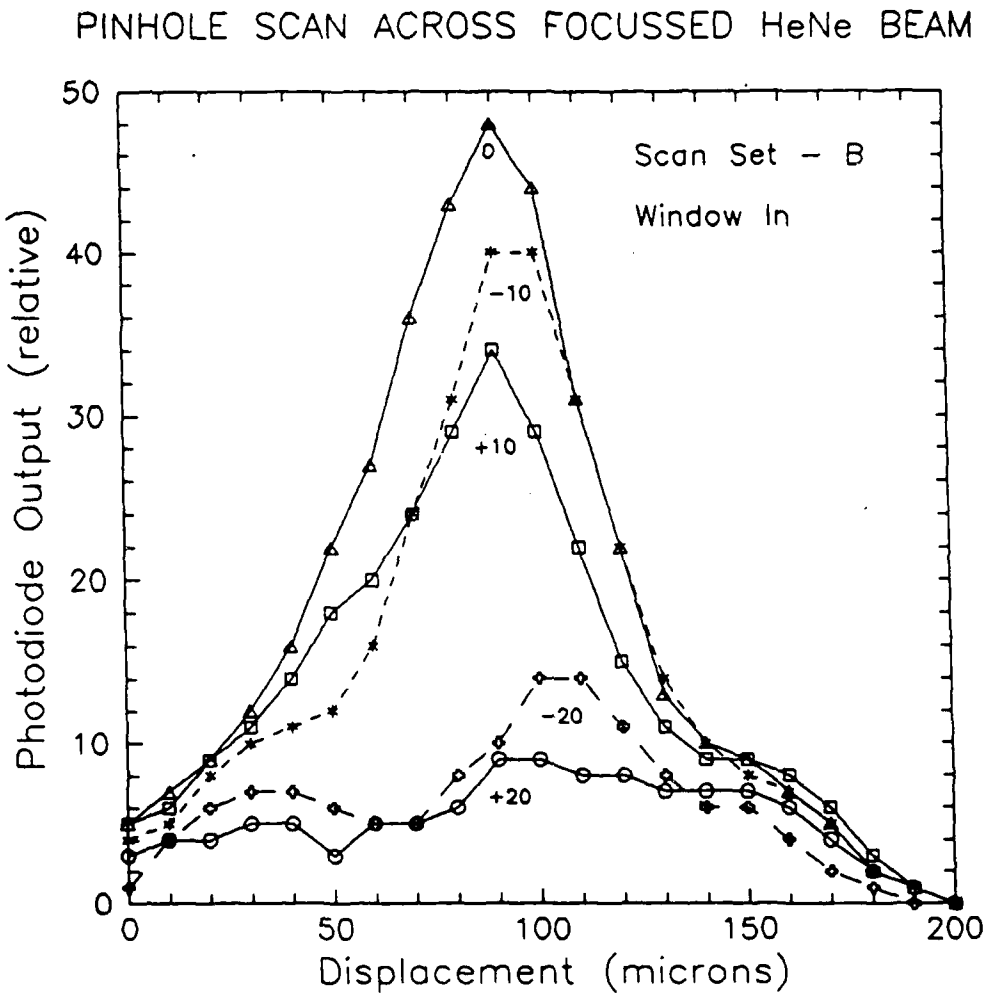

Figure 4. Intensity profile of focused laser spot with a window in the laser beam path - first alignment. Horizontal displacement is shown on the horizontal axis. Vertical displacement in 20 micron increments is shown by the individual labeled curves.

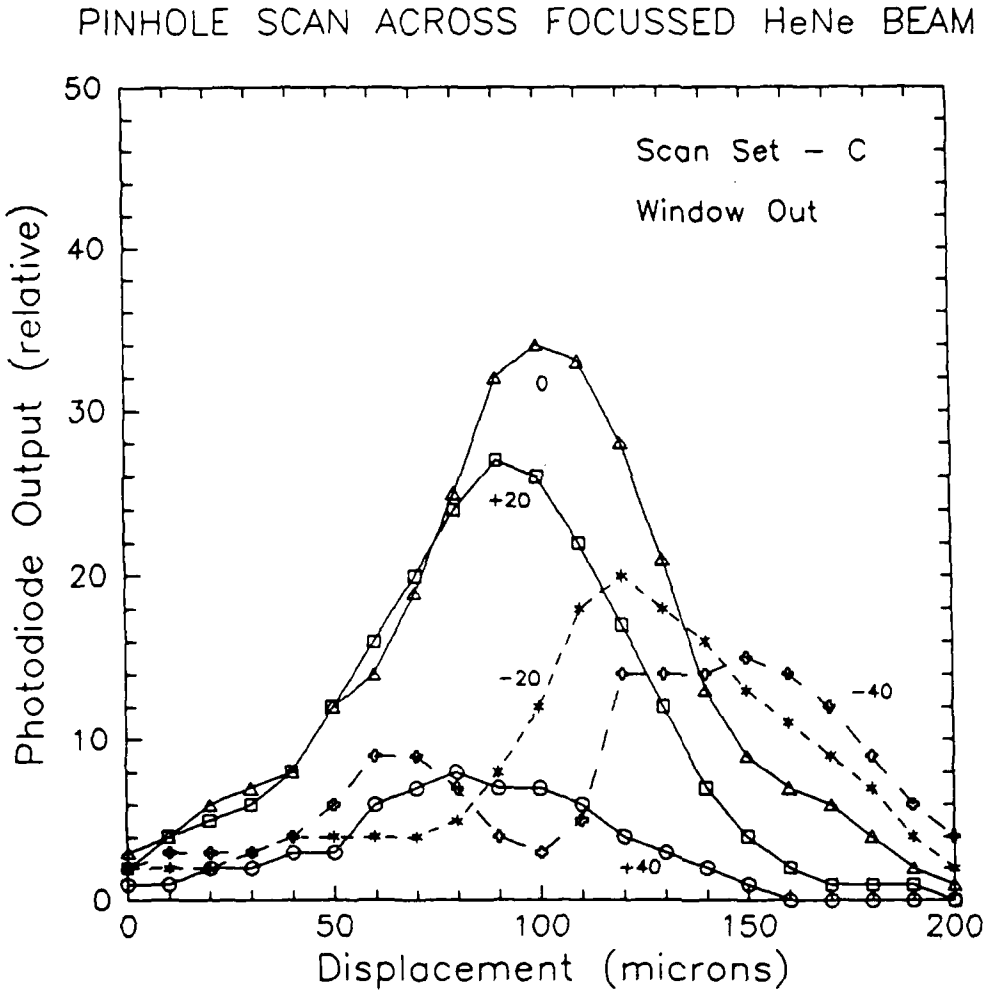

Figure 5. Intensity profile of focused laser spot with no window in the laser beam path - second alignment. Horizontal displacement is shown on the horizontal axis. Vertical displacement in 20 micron increments is shown by the individual labeled curves.

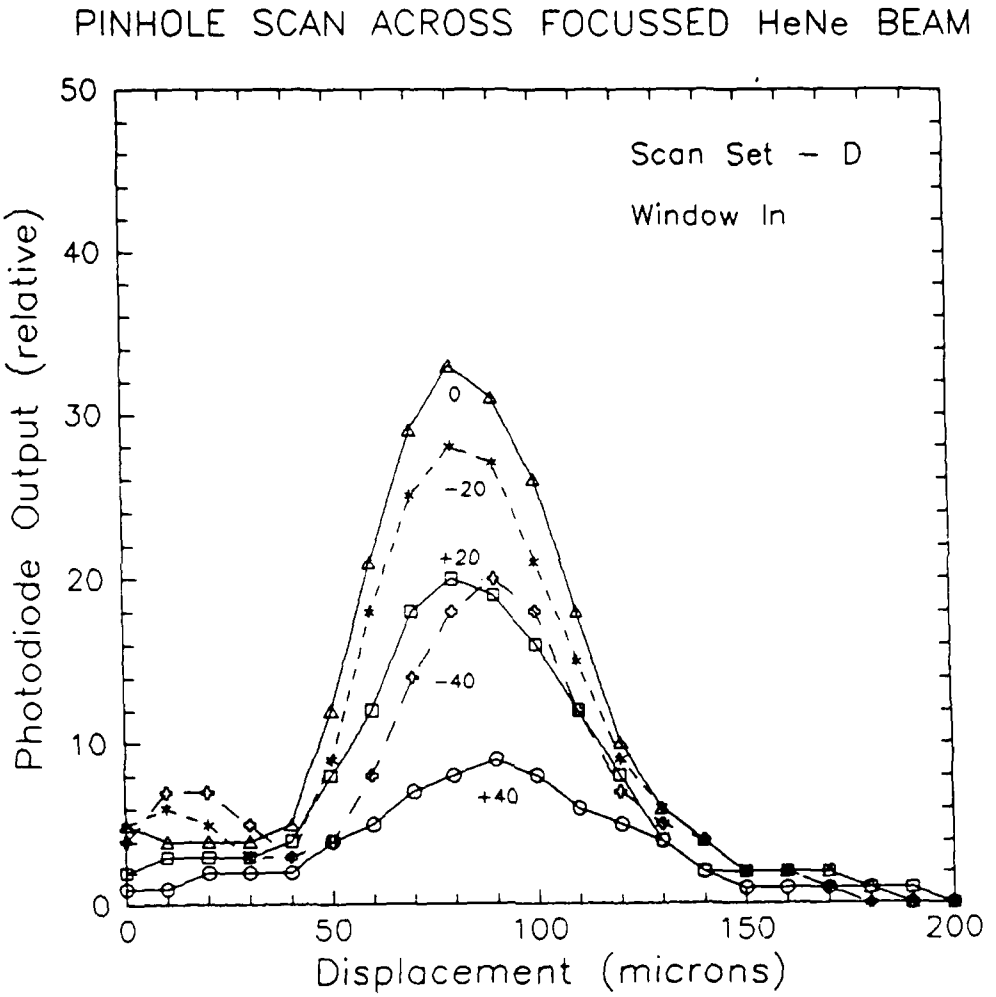

Figure 6. Intensity profile of focused laser spot with a window in the laser beam path - second alignment. Horizontal displacement is shown on the horizontal axis. Vertical displacement in 20 micron increments is shown by the individual labeled curves.

were repeated. Figures 5 and 6 show the spot profile without and with the window, respectively, after realignment. The profiles show that the full width of the laser beam is approximately 150 microns, consistent with the computed diameter. The profiles also show that the spot is not necessarily symmetrical, and can contain secondary peaks.

5.0 ESTIMATED ALIGNMENT UNCERTAINTY WHEN USING THE SINGLE EVENT UPSET - VAN DE GRAAFF ALIGNMENT SYSTEM

When the pinhole and the device under test are aligned using this new alignment system, as detailed in Section 2.1, the irreducible uncertainty in alignment consists of two parts. The first part is the uncertainty in centering the device under test in the laser spot, and the second part is the uncertainty in centering the pinhole in the laser beam. These two uncertainties will be estimated below.

The measured laser spot profiles in Section 4.2 show that the half width of the laser spot at half maximum intensity is approximately 30 microns. This value of 30 microns can be taken as a conservative estimate of the accuracy to which the device under test can be centered in the laser spot. The pinhole is centered in the laser beam using the photodiode and electronic display, and therefore it should be possible to center the pinhole in the laser beam with an accuracy of better than 30 microns. Taking into account the typical asymmetry of the laser spot, as shown in Figures 3 through 6, a conservative estimate of the uncertainty in aligning the pinhole in the laser beam is 20 microns. Therefore, the estimated total uncertainty in the alignment using the new system is the sum of these two contributions, or 50 microns.

APPENDIX 1. BASIC OPTICS OF LASER RESONATORS

This appendix is reproduced from Lasers and Applications, October 1984. The article contains a useful discussion of the propagation of laser beams.

Basic Optics of Laser Resonators

Effective Use of Lasers is Simplified by Knowledge of Gaussian Laserbeams

by James T. Luxon

An earlier article [*L&A* Jun p97] dealt with introductory concepts of geometrical and physical optics and their application to lasers. This article, based heavily on that earlier piece, deals with the nature of Gaussian laserbeams, including their behavior in the laser itself, propagation through space, focusing, and depth of focus. Lowest order, or fundamental Gaussian and higher-order Gaussian beams will be considered.

The high degree of coherence of laserbeams and the unique way they are generated produce propagation and focusing properties quite unlike those of conventional light sources. In the ideal case, the phasefronts produced by lasers are spherical (at least, near the axis). They appear to originate from a point source; consequently, the geometrical image produced by a focusing element is a point. Diffraction effects, however, limit the spot size to a finite value, hence the term "diffraction-limited focusing." Such ideal cases provide excellent approximations to many real-world laser applications and serve as a basis for understanding the non-ideal cases.

Jim Luxon is professor of materials science at the GMI Engineering & Management Institute, Flint MI

Laser Resonators

Laser resonators (also called optical cavities) fall into two categories: stable and unstable. Stable resonators are ones in which some rays perpetually retrace themselves (if we ignore the effects of transmission through the mirrors). Unstable resonators are those in which the rays do not retrace themselves and simply "walk off" the axis and out of the cavity. Figure 1 illustrates these two cases. Note that in the unstable resonator the output is the *result* of geometrical walkoff, but that diffraction produces a substructure in the output. Although unstable resonators are common in high-power lasers, they will not be discussed further here.

It is a simple matter to determine if a resonator is stable. To do so, we define the parameters $g_1 = 1 - L/r_1$ and $g_2 = 1 - L/1r_2$, where L is the optical resonator length and r_1 and r_2 are the radii of curvature of the back and output mirrors, respectively. Note that L is the optical length of the cavity, not its geometrical length. The optical length of any transmissive element in the cavity

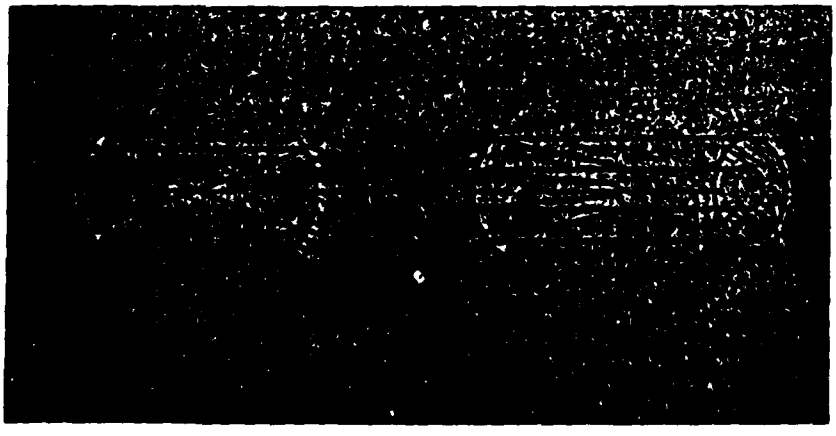

Figure 1. (a) Stable confocal resonator; (b) unstable confocal resonator.

equals nl, where l is the element's thickness and n is its refractive index. This stems from the fact that the wavelength of light is shorter in dielectric materials than in free space. A laser resonator is stable if it satisfies the criterion $0 \leq g_1 g_2 \leq 1$; otherwise, it is unstable. A simple way to express this is: "Either the center of curvature of one mirror or that mirror itself, but not both, must cut the axis between the other mirror and its center of curvature."[1] It doesn't matter which mirror you apply this definition to.

A laserbeam generated in a resonator with two spherical mirrors is illustrated in Figure 2. The lines representing the laserbeam are *not* rays; instead, they are the loci of points representing the beam radius, w. Note that the beam has a waist where the radius is designated w_o. This waist is usually located inside the laser cavity or at the output mirror. Its location, z_2, is determined by purely geometrical factors[2] as

$$z_2 = \frac{g_1 (1 - g_2) L}{g_1 + g_2 - 2 g_1 g_2} \qquad (1)$$

For a flat output mirror, $g_2 = 1$ and $z_2 = 0$. For two flat mirrors, the output is aperture-limited and Equation 1 is not meaningful.

The typical laser resonator can support many modes of oscillation. The so-called axial or Fabry-Perot oscillation modes occur because the phase change in one complete round trip in the cavity must be an integral multiple of 2π. Stated another way, the mirrors must be an integral number of halfwaves apart, so that $n(\lambda/2) = L$. This requirement produces a frequency spacing of $c/2L$ between axial modes, where c is the speed of light. If L is 30 centimeters, the axial modes are separated by 500 megahertz. This is small enough that most visible-wavelength lasers may operate in several axial modes.

In addition to axial modes, transverse electromagnetic (TEM_{pq}) modes also occur. The TEM_{pq} modes are any spherical phasefront distribution that is self-reproducing upon one complete round trip in the cavity. Some representative transverse modes are depicted in Figure 3, where the subscripts represent the number of orthogonal nodes. TEM_{00} is the lowest order transverse mode, frequently referred to as the Gaussian mode. The TEM_{10}^* mode is the so-called "doughnut" mode, which can be thought of as a superposition of

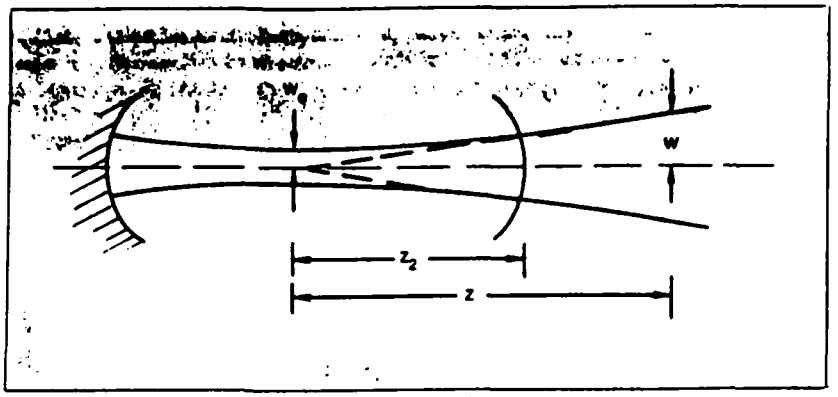

Figure 2. Laserbeam propagation from a cavity with two spherical mirrors. Any lensing effects from the output coupler have been neglected in this diagram.

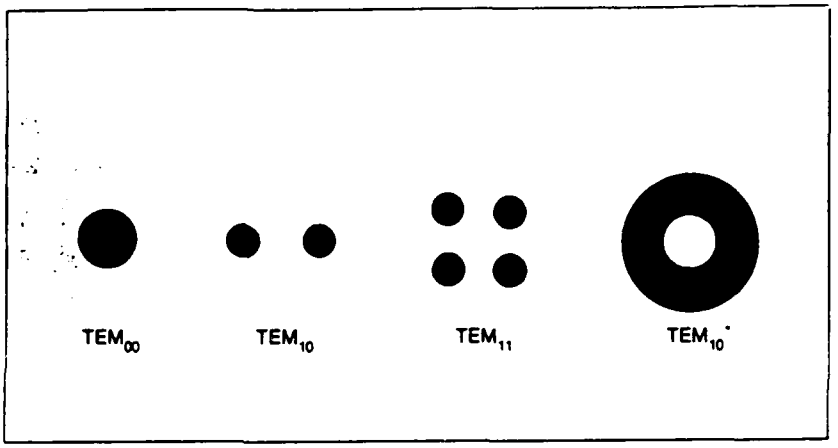

Figure 3. Sample TEM_{pq} mode profiles.

TEM_{10} and TEM_{01} modes, or a TEM_{10} mode in which the node orientation is changing with time.

The modes in Figure 3 are rectangular; circular modes may also occur. We will stick to discussing rectangular modes here, because they are more mathematically tractable than circular modes. Furthermore, they occur frequently in real lasers. Finally, the circular modes can be mathematically represented as a sum of rectangular modes.

The TEM_{00} mode is characterized by a purely Gaussian irradiance distribution (Figure 4) given by

$$I = I_0 e^{\frac{-2r^2}{w^2}} \qquad (2)$$

where I_0 is irradiance on the beam axis, r is distance measured from the axis, and w is the radius. This radius is defined such that $I = I_0/e^2$ at $r = w$. Other definitions of beam radius are sometimes encountered, but they can be mathematically related to this $1/e^2$ definition.

All higher-order modes contain a Gaussian term of the form given by Equation 2. The Gaussian radius is the same for *all* modes for a given laser. However, the $1/e^2$ or Gaussian radius is of no practical value for higher-order modes.

Two useful facts concerning the TEM_{00} mode are evident from Figure 4. First, the irradiance at $r = w$ is 0.135 I_0. Second, the total power contained in a spot of radius $r = w$ is 0.865 times the total power.

Figure 5 is a plot of irradiance versus a linear dimension for a rectangular higher-order mode. The coordinate x is in either of the two directions orthogonal to the nodes. If this mode were symmetrical (such modes frequently are not), it would be a TEM_{44}. The beam size, X, is taken as half the outer peak-to-peak distance, because this distance is directly measurable from an image of the beam or irradiance profile measurements.

Beam Waist and Propagation

As noted earlier, all ideal laserbeams from lasers with spherical mirrors are Gaussian, and the

Gaussian radius is the same from all modes of a given laser. Accordingly, it is simplest to discuss the TEM_{00} mode first and then extend the results to higher-order modes.

Referring to Figure 2, the waist shown has a size dependent on both diffraction and geometrical factors. The Gaussian radius is given by[2]

$$w_o = \left(\frac{\lambda L}{\pi}\right)^{1/2} \frac{|g_1 g_2 (1 - g_1 g_2)|^{1/4}}{|g_1 + g_2 - 2g_1 g_2|^{1/2}} \quad (3)$$

where λ is the wavelength of the light. This expression is indeterminate for the symmetrical confocal resonator ($g_1 = g_2 = 1$), but a simple derivation yields $w_o = |\lambda L/(2\pi)|^{1/2}$ for this case. Also, Equation 3 is meaningless for the case of two flat parallel mirrors, because the beam size is determined by the limiting aperture. But for other stable cavity configurations, Equation 3 yields useful values for w_o.

The phasefronts, uniphase for the TEM_{00} mode, are spherical near the axis with the radius of curvature given by

$$R = z\left(1 + (z_R/z)^2\right) \quad (4)$$

Here, z_R is the Rayleigh range and, for the TEM_{00} mode, is given by $z_R = \pi w_o^2/\lambda$. Since w_o is the same for *all* modes, z_R and R are likewise the same for *all* modes. The Rayleigh range is the distance from the waist at which the radius of curvature of the phasefront is a *minimum*. From Figure 2, the locus of points representing the beam radius becomes asymptotic to straight lines that intersect at a point located at the waist. This is the far-field condition. For the near-field condition, the point is located to the left of the waist.

Gaussian modes of any order *do not* change form as a result of propagation in free space; they only change size. However, propagation through inhomogeneous media will distort the modes.

The radius of a propagating beam as a function of distance z from the waist is given by[2]

$$w = w_o\left(1 + (z/z_R)^2\right)^{1/2} \quad (5)$$

The output mirror will act as a lens unless its surfaces have identical curvatures. Thus, in general, a virtual waist size and location must be computed to apply Equation 5 correctly. The far-field condition is approached as z becomes much larger than z_R. For a small helium-neon laser z_R is about 1 meter, so the far-field condition becomes applicable about 50 m from the laser head. The beam divergence in the far field, θ_{ff}, is given by

$$\theta_{ff} = w_o/z_R \quad (6)$$

Whereas z_R is independent of mode, the far-field divergence or diffraction angle depends on how the spot size is defined.

Focusing Gaussian Beams

A thin lens transforms a spherical phasefront according to

$$\frac{1}{R_1} + \frac{1}{R_2} = \frac{1}{f} \quad (7)$$

where R_1 is the radius of curvature of the wave incident on the lens and R_2 is the radius of curvature of the transmitted phasefront. The beam diameter is assumed equal immediately on either side of the lens. R_1 is positive if the beam is diverging (real object), and R_2 is positive if the beam is converging (real image). Otherwise, they are negative. Equation 7 can be used with Equation 4 to compute the transformation of the radius of curvature by a thin lens.

An equation resembling the thin lens equation can be written to relate waist location of a beam incident on a thin lens to the location of the transformed waist produced by the lens[3] (Figure 6).

$$\frac{1}{S + \frac{z_R^2}{S - f}} + \frac{1}{S'} = \frac{1}{f} \quad (8)$$

In Equation 8, S is the distance of the incident beam waist from the lens and S' is the distance of the transformed waist from the lens. S is positive if on the left, S' is positive if on the right, and f is positive if the lens is a converging lens (thicker in the middle than at the edges). The thin lens magnification m becomes

$$m = 1/|(1 - S/f)^2 + (z_R/f)^2|^{1/2} \quad (9)$$

The transformed waist size can be computed from Equation 9. Equation 5 can then be applied to the new waist, taking the origin for z at the location of the new waist.

A HeNe laser operating in the TEM_{00} mode with $z_R = 1$ m and its waist located 2 m from a thin lens with a 5-cm focal length will produce a focused spot at $S' = 5.1$ cm. If we assume an initial waist radius of 0.5 mm, the focused spot will have a radius of 0.011 mm.

A simple way to estimate focused spot size is to assume that, because of small beam divergence, the beam is focused in the focal plane of the lens. With this assumption, Equation 5 can be applied directly. Substituting $z = f$, $w = w_L$, and $z_R = \pi w_o^2/\lambda$ and neglecting the "1" term relative to $(f/z_R)^2$, we get

$$w_O = \frac{\lambda f}{\pi w_L} \quad (10)$$

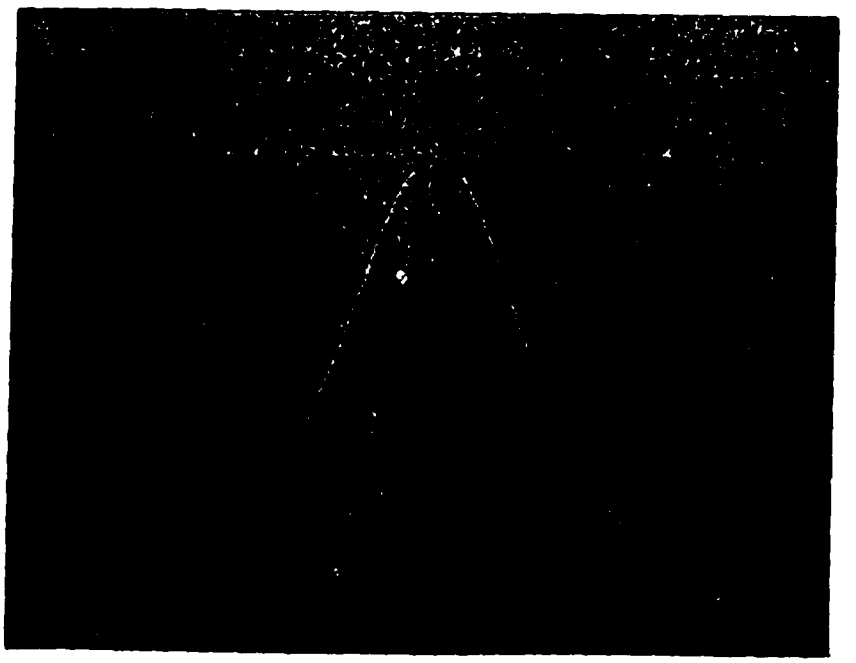

Figure 4. Profile of a TEM_{00} beam.

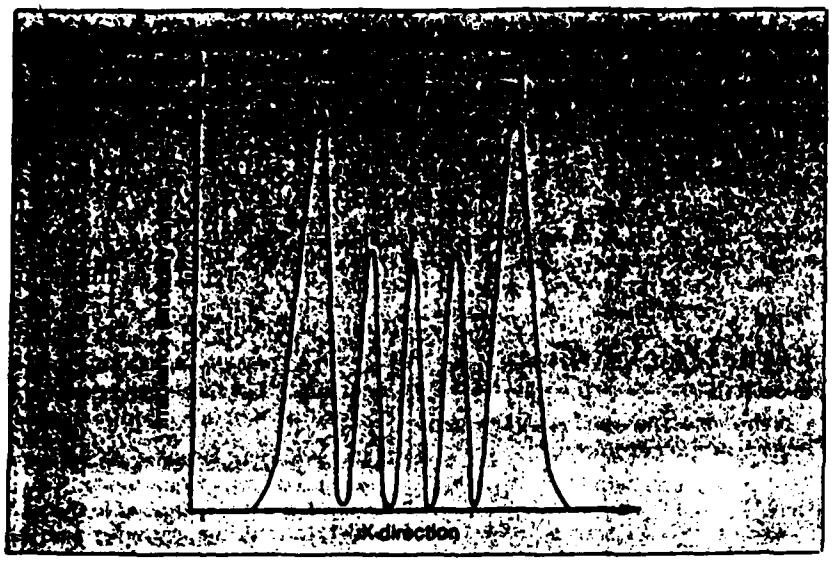

Figure 5. Power density for an arbitrary higher-order mode (in one dimension orthogonal to the nodes of the modal pattern).

Equation 10 is apparently the source of the familiar equation for spot size $w_o = f\Theta$. However, $\lambda/\pi w_L$ is not the divergence angle. It will be the far-field divergence angle *if* w_L equals the laser waist radius. That can be approximately true only if the lens is close to the laser, in which case the actual divergence angle may be close to zero and is most certainly much less than Θ_{ff}. Equation 10 is more frequently useful for single-element focusing of a laserbeam than is Equation 9, because we seldom know the actual laser waist size.

In laser applications where focusing is applied, we must know the allowable variation in distance from the point of best focus. This is the depth of focus (frequently incorrectly referred to as the depth of field). It depends on how much spot size variation can be tolerated in a particular application. Equation 5 can be applied to deduce a useful definition of depth of focus. Let $z = d$ and $w = \varrho w_o$, where ϱ determines the amount by which w can vary from w_o. Solving Equation 5 with these substitutions yields

$$d = \pm\pi\sqrt{\varrho^2 - 1}\ \frac{w_o^2}{\lambda} \qquad (11)$$

For $\varrho = 1.05$ (5% variation in spot size), this reduces to the often-stated depth of focus relation $d = \pm 0.32\pi w_o^2/\lambda = \pm w_o^2/\lambda$. Equation 11 is, however, more generally useful. A HeNe laser focused to a 0.011-mm spot (radius) will have a depth of focus of 0.28 mm for $\varrho = 1.1$ (10% change in spot size).

Extending to Higher-Order Modes

These equations are valid for Gaussian beams of all mode structures. However, the usual definitions of Gaussian beam spot size, such as the e^{-2} definition used here, are not practical for higher-order-mode beams. For such higher-order modes, it is virtually impossible to measure such a spot size. The spot size definition for higher-order-mode beams illustrated in Figure 5 is measurable and can be easily related to other definitions, if necessary.

The process for modifying these equations to apply to higher-order modes begins with replacing w_o with $2^{1/2}\sigma_o$. Here, σ_o is the point where the irradiance is e^{-1} of its value at the center of a TEM_{00} beam. This leads to a spot size definition for rectangular Gaussian beams given by[4]

$$\sigma_p = (2p + 1)^{1/2}\sigma_o \qquad (12)$$

where σ_p is related to the standard deviation of the irradiance profile. This definition of spot size is always greater than X (from Figure 5) and is therefore difficult, if not impossible, to measure. However, X is related to σ_p by $X^5\ k_p^9\sigma_p$, where k_p can be numerically evaluated.[5,6] Approximate values of k_p are given by

$$k_p = 1 + 0.73e^{-0.78p} \qquad (13)$$

The waist size in the laser becomes[7]

$$X_o = \left(\frac{\lambda L(2p + 1)}{2\pi k_p^2}\right)^{1/2} \times \frac{|g_1g_2(1 - g_1g_2)|^{1/4}}{|g_1 + g_2 - 2g_1g_2|^{1/2}} \qquad (14)$$

The Rayleigh range is a purely geometrical quantity, but it is frequently convenient to express it in terms of waist size

$$z_R = 2\pi k_p^2 X_o^2/(\lambda(2p + 1)) = L\,\frac{|g_1g_2(1 - g_1g_2)|^{1/2}}{|g_1 + g_2 - 2g_1g_2|} \qquad (15)$$

The beam propagation equation then becomes

$$X = X_o\left(1 + \left(\frac{\lambda z(2p + 1)}{2\pi k_p^2 X_o^2}\right)^2\right)^{1/2} \qquad (16)$$

The focused spot size, assuming the spot is located in the focal plane, becomes

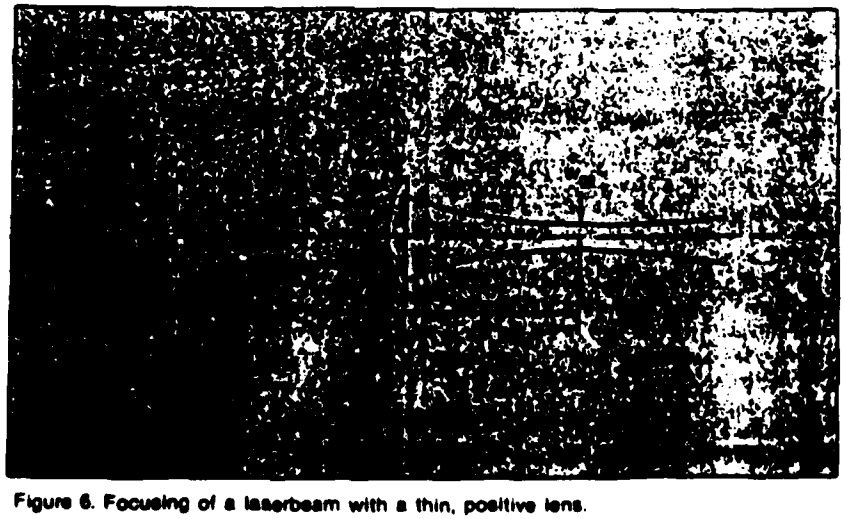

Figure 6. Focusing of a laserbeam with a thin, positive lens.

$$X_o = \frac{\lambda f (2p + 1)}{2\pi k_p^2 X_L} \qquad (17)$$

and the depth of focus is given by

$$d = \pm 2\pi \sqrt{\rho^2 - 1}\, k_p^2 X_o^2 / (2p + 1)\lambda \qquad (18)$$

Equations similar to these can be written for the radius of circular (Laguerre-Gaussian) higher-order modes by setting kp = 1 and replacing (2p + 1) with 2(2p + m + 1), where *p* and *m* are the number of radial and angular nodes, respectively.[8] This definition of spot radius can be related to the fraction of power transmitted through a circular aperture of this radius.

Conclusion

These equations are accurate and simple to use with a programmable calculator. But even a near-ideal laserbeam truncated by an aperture will not obey these equations. Also, many lasers produce far-less-than-ideal Gaussian beams, because of truncations or inhomogeneities within the cavity. Nevertheless, this material represents an essential starting point for understanding the behavior of laserbeams.

All other things being equal, higher-order-mode laserbeams have larger waists, diverge faster because of diffraction, focus to larger spots, and have shorter depth of focus because of greater diffraction spreading than their lower-order counterparts. Many of these shortcomings can be overcome by resonator design or external optics, generally at the cost of larger beam size (Figure 6).

Why do higher-order-mode beams suffer more from diffraction effects than TEM_{00} beams? Remember that diffraction spreading is inversely proportional to aperture size. But the effective aperture for higher-order-mode beams is approximately the size of the individual spots, rather than the overall beam size. Indeed, that is the reason for the (2p + 1) factor in the spot size definition. This also explains why ordinary light beams spread much more rapidly than laserbeams: The effective aperture is extremely small because of the lack of coherence (definite phase correlation) between different parts of the cross-section of an ordinary light beam. □

References

1. A. Yariv, *Quantum Electronics*, John Wiley & Sons Inc., New York (1968).
2. H. Kogelnik and T. Li, "Laser Beams and Resonators," *Appl. Opt.* **5**:1550-1567 (October 1966).
3. S. Self, "Focusing of Spherical Gaussian Beams," *Appl. Opt.* **22**:658-661 (1 March 1983).
4. W. Carter, "Spot Size and Divergence for Hermite Gaussian Beams of Any Order," *Appl. Opt.* **19**:1027-1029 (1 April 1980).
5. J. Luxon and D. Parker, "Practical Spot Size Definition for Single Higher-Order Rectangular Mode Laser Beams," *Appl. Opt.* **20**:1728-1729 (15 May 1981).
6. J. Luxon and D. Parker, "Higher-Order CO_2 Laser Beam Spot Size and Depth of Focus Determination," *Appl. Opt.* **20**:1933-1935 (1 June 1981).
7. J. Luxon, J. D. Parker, and J. Karkheck, "Waist Location and Rayleigh Range for Higher-Order Mode Laser Beams," *Appl. Opt.* **23**:2088-2090 (1 July 1984).
8. R. Phillips and L. Andrews, "Spot Size and Divergence for Laguerre-Gaussian Beams of Any Order," *Appl. Opt.* **22**:643-644 (1 March 1983).

APPENDIX 2. OPERATING PRINCIPLE AND DIMENSIONAL DRAWING OF THE QUADRANT PHOTODIODE

This appendix is reproduced from the Hamamatsu Position-Sensitive Detectors Data Book. The first part contains a discussion of the operating principle and characteristics of the quadrant photodiode. The second part shows the dimensional diagram of the type S1743 quadrant photodiode used in the single event upset - Van de Graaff alignment system.

The position-sensitive detector (PSD) is an optoelectronic sensor that provides continuous position data of a light spot travelling over its surface. Compared to the discrete element detectors such as CCD, the PSD features high position resolution, fast response speed, and simple operating circuits.

STRUCTURE

As shown in Fig.a., a sectional structure view, the PSD consists of three layers: P-layer, N-layer underneath, and I-layer in between all placed, over a planar silicon substrate. Incident light falling on the PSD is converted photoelectrically and detected by the two electrodes on P-layer (P- and N-layers for duo-lateral types) as photocurrent.

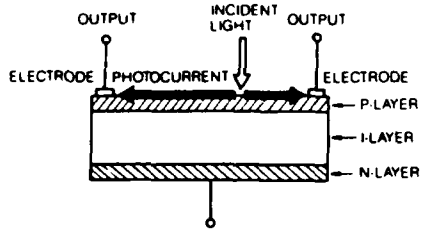

Fig. a. PSD sectional view

PRINCIPLE

When a light spot falls on the PSD, an electric charge proportional to the light energy is generated at the incident position. This electric charge is driven through the resistive P-layer and collected by the electrodes. Since the resistivity of the P-layer is uniform, the photocurrent collected by an electrode is inversely proportional to the distance between the incident position and the electrode. It is possible to obtain the following formulas for the photocurrents I_1 and I_2 collected by the electrodes, where 2L and I_0 respectively stand for the electrode interdistance and the total photocurrent.

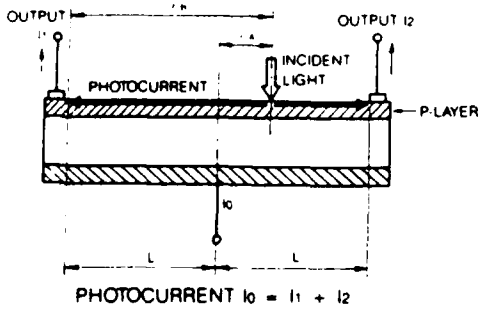

- **When the center point of the PSD is set at the original point:**

$$I_1 = I_0\frac{L - xA}{2L} \quad \cdots\cdots (1) \qquad I_2 = I_0\frac{L + xA}{2L} \quad \cdots\cdots (2)$$

$$\frac{I_2 - I_1}{I_1 + I_2} = \frac{xA}{L} \quad \cdots\cdots (3) \qquad \frac{I_1}{I_2} = \frac{L - xA}{L + xA} \quad \cdots\cdots (4)$$

- **When the end of the PSD is set at the original point:**

$$I_1 = I_0\frac{2L - xB}{2L} \quad \cdots\cdots (5) \qquad I_2 = I_0\frac{xB}{2L} \quad \cdots\cdots (6)$$

$$\frac{I_2 - I_1}{I_1 + I_2} = \frac{xB - L}{L} \quad \cdots\cdots (7) \qquad \frac{I_1}{I_2} = \frac{2L - xB}{xB} \quad \cdots\cdots (8)$$

By finding the difference or ratio of I_1 and I_2 thereby, the incident position of light can be found by the formulas (3), (4), (7) and (8) irrespective of the energy of incident light.

ONE-DIMENSIONAL PSD

The PSD is classified into two types: for one-dimensional position detection and two-dimensional position detection. Fig. b shows the structure of the one-dimensional PSD.

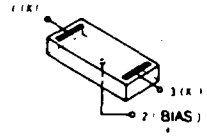

Fig. b. Structure

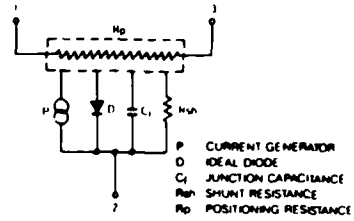

Fig. c. Equivalent circuit

Fig. c. is an equivalent circuit of the relation between the uniformly distributed current dividing resistive layer and corresponding electrodes of the one-dimensional PSD. Since the PSD has the distribution circuits Cj and Rp, its time constant acts as a decisive element for waveform response. By using a position signal integration circuit, however, the one dimensional PSD can be used for position detection of a laser beam of 100ps pulse width.

TWO-DIMENSIONAL PSD

The two-dimensional PSD is classified by structure into two types: duo-lateral type and tetra-lateral type.

- **Duo-Lateral Type**

As shown in Fig. d., the duo-lateral type has electrodes on both surfaces (upper surface and under surface) of a photodiode. As shown in the equivalent circuit in Fig. e., each position signal (photocurrent) is only divided into two parts by two resistive layers, and therefore, this type has a high position detecting ability (smaller position detection error and higher resolution)

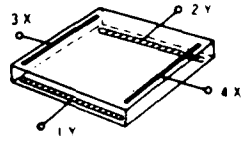

Fig. d. Structure (Duo-Lateral Type)

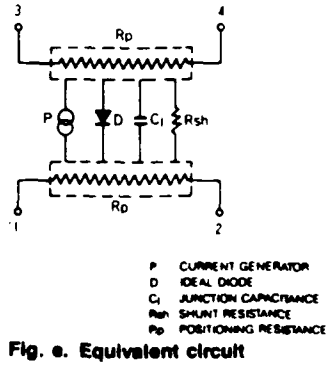

Fig. e. Equivalent circuit (Duo-Lateral Type)

- **Tetra-Lateral Type**

As shown in Fig. f., this type has 4 electrodes on the upper surface of a photodiode. Photocurrent is divided into 4 parts by the same resistive layer and output as a position signal. (See Fig. g.) As compared with the duo-lateral type, this type has a distortion that is greater in the circumference. However, it features a bias that can be applied easier, a dark current that is smaller, and a response time that is faster.

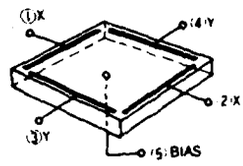

Fig. f. Structure (Tetra-Lateral Type)

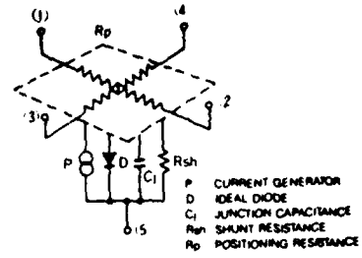

Fig. g. Equivalent circuit (Tetra-Lateral Type)

• Pin-Cushion Type (Improved Tetra-Lateral Type)
This is the improved tetra-lateral type, with the improved sensitive surface and electrodes. In addition to small dark current, fast response and easy bias application, which are advantages of the tetra-lateral type, distortion in the circumference has been greatly reduced.

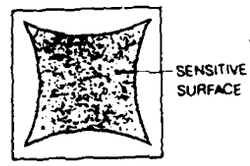

Fig. h. Shape of sensitive area

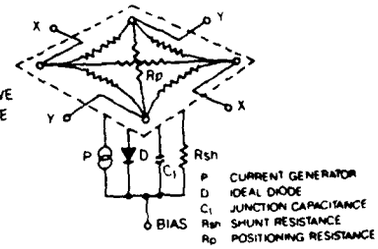

Fig. i. Equivalent circuit

CONVERSION FORMULAS

The position of the light spot on the PSD can be found by the following formulas, whereas X_1, X_2, and Y_1, Y_2 represent the output signals (photocurrent) of each electrode, and x, y are the coordinate positions of the light spot.

• One-Dimensional PSD

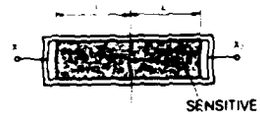

$$\frac{X_2 - X_1}{X_1 + X_2} = \frac{x}{L}$$

• Two-Dimensional PSD (Square type)

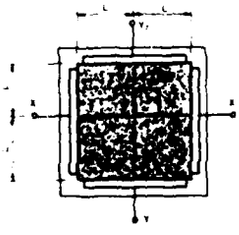

$$\frac{X_2 - X_1}{X_1 + X_2} = \frac{x}{L}$$

$$\frac{Y_2 - Y_1}{Y_1 + Y_2} = \frac{y}{L}$$

• Two-Dimensional PSD (Pin-Cushion type)

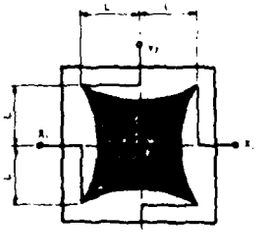

$$\frac{(X_2 + Y_1) - (X_1 + Y_2)}{X_1 + X_2 + Y_1 + Y_2} = \frac{x}{L}$$

$$\frac{(X_2 + Y_2) - (Y_1 + Y_1)}{X_1 + X_2 + Y_1 + Y_2} = \frac{y}{L}$$

⑧ S1743

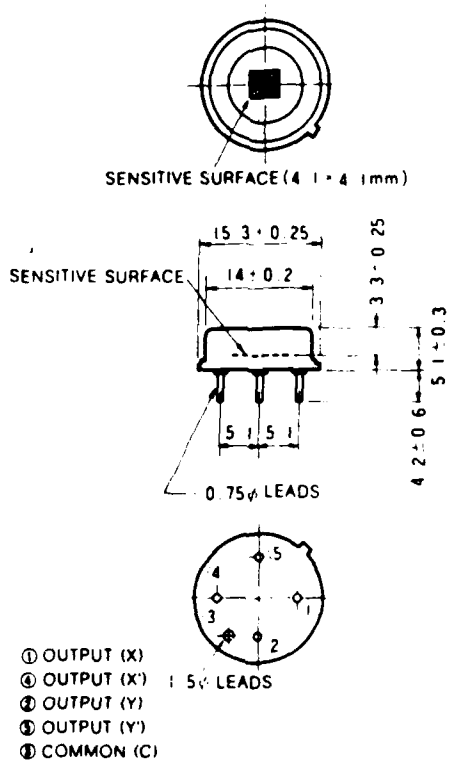

① OUTPUT (X)
④ OUTPUT (X')
② OUTPUT (Y)
⑤ OUTPUT (Y')
③ COMMON (C)

Net weight: 3g


FILMED
48